Supporting Information for Toward Confined Carbyne with Tailored Properties

Lei Shi,[*,†] Ryosuke Senga,[‡] Kazu Suenaga,[‡] Hiromichi Kataura,[‡] Takeshi Saito,[‡] Alejandro Pérez Paz,[*,¶,§] Angel Rubio,[*,§,∥,⊥] Paola Ayala,[#] and Thomas Pichler[*,#]

†*School of Materials Science and Engineering, State Key Laboratory of Optoelectronic Materials and Technologies, Nanotechnology Research Center, Sun Yat-sen University, Guangzhou 510275,P. R. China*

‡*Nanomaterials Research Institute, National Institute of Advanced Industrial Science and Technology, Tsukuba 305-8565, Japan*

¶*Chemistry Department, United Arab Emirates University, P.O. Box 15551, Al Ain, United Arab Emirates*

§*Nano-Bio Spectroscopy Group, Departamento de Fisica de Materiales, University of the Basque Country, Donostia-San Sebastián 20018, Spain*

∥*Max Planck Institute for the Structure and Dynamics of Matter, Center for Free Electron Laser Science, 22761 Hamburg, Germany*

⊥*Center for Computational Quantum Physics, Simons Foundation Flatiron Institute, New York,New York 10010, United States*

#*Faculty of Physics, University of Vienna, Vienna, Austria.*

E-mail: shilei26@mail.sysu.edu.cn; aperez@uaeu.ac.ae; aperez@uaeu.ac.ae; thomas.pichler@univie.ac.at

Phone: +86-20-43111460, +43-1-4277-51466

The eDIPS SWCNTs with different average diameter were annealed at different temperatures to figure out the optimized temperature for synthesis of the CCs. Fig. S1 displays the Raman spectra of annealed eDIPS-1.3 nm at different temperature. It is clearly seen that the peaks between 250 and 350 cm^{-1} corresponding to inner tubes increase with the temperature. In addition, the CC-band consisting of several components can be observed using multi-frequency lasers as excitations (Figs. S2 and S3). As for the eDIPS-1.0 nm SWCNTs, the optimal temperature is higher than that of eDIPS-1.3 nm and eDIPS-1.7 nm SWCNTs (Figs. S4 and S5). Obvious changes of the RBM peaks relate to the diameter changes of the CNTs. As shown in Fig. S4, the Raman peaks at around 240 cm^{-1} correspond to the SWCNTs with diameter around 1 nm. The peaks decrease with the increased annealing temperature, and new peaks at around 160 cm^{-1} appear, suggesting that the SWCNTs were enlarged during the annealing. Also, the peaks between 260 and 320 cm^{-1} corresponding to thin SWCNTs disappear when annealed at 1300 and 1350 °C due to enlargement, however, arise again at 1400 °C and above because of the new formed inner tubes inside the enlarged SWCNTs. Therefore, higher temperature is needed for the enlargements of the SWCNTs and the formation of the inner tubes as well as the CCs. The multi-frequency Raman spectra shown in Figs. S6

and S7 demonstrate again that no long CCs can be found in the annealing eDIPS-1.0 nm SWCNTs, indicating the uniform length of the synthesized intermediate CCs. For comparison, although very little long CCs exist in the eDIPS-1.7 nm SWCNTs, the main component is indeed short CCs. Therefore, the eDIPS-1.3 nm SWCNTs is the best for formation of long CCs (Figures 2 and 3 in the main text). Finally, as shown in Fig. S8, the semiconducting SWCNTs produced more thin inner tubes than the metallic SWCNTs after annealing, resulting in more CCs at low Raman frequency in the CC-band.

CC polymerization affected by the diameter:

By reducing the CNT diameter, one also reduces the entropy cost for polymerization and hence renders this reaction more thermodynamically favorable. As in any gas-phase polymerization, the CC formation has an intrinsic negative reaction entropy, ΔS=$S(CC)$-$S(R) < 0$, where R denotes the precursors. According to the Sackur-Tetrode equation of statistical mechanics, the entropy is proportional to the logarithm of the container volume (and therefore on the CNT diameter D): S $\sim k_B \cdot \ln(D)$. Assuming all other factors equal and same initial and final compositions, the difference between reaction entropies for CC polymerization in a thin (t) and wide (w) CNT is $\Delta\Delta S^\circ = \Delta S_t^\circ$ - ΔS_w° = $S_t^\circ(CC)$ - $S_t^\circ(R)$ - $[S_w^\circ(CC)$ - $S_w^\circ(R)] \sim S_w^\circ(R)$ - $S_t^\circ(R) = Nk_B \cdot \ln(D_w \,/\, D_t) > 0$, which means that $\Delta S_t^\circ > \Delta S_w^\circ$, where k_B is the Boltzmann constant and N is the number of precursor carbon monomers R. Here, we made the approximation of canceling the entropy contributions from the CC products since $S_t^\circ(CC) \approx S_w^\circ(CC)$. Thus, the CC synthesis is more facile inside thin CNTs, where precursors are less "dilute" than in wide CNTs. This can also be obtained simply from the Law of mass action, $K_t = K_w \cdot (D_w \,/\, D_t)$, where K is the equilibrium constant or from the thermodynamic relation ΔG° = - $RT \cdot \ln K$.

Full Computational Details: All molecular dynamics (MD) simulations used the AIREBO force field[1] as implemented in the LAMMPS code.[2] AIREBO is a reactive force field suited to study chemical reactions in large carbonaceous systems. The typical simulated system consisted of 20 unit cells of an undefected chiral (6,4) SWCNT (152 atoms/per unit cell, a total 3040 C atoms) containing an array of C atoms inside randomly placed along the tube main axis (z axis). For an equilibrium AIREBO nanotube C-C distance of 1.402 $\mathring{A}$, the mean diameter and total length of the (6,4) SWCNT was 6.74 and 366.78 $\mathring{A}$, respectively, whereas for the (20,0) SWCNT it was 15.7 and 364.3 $\mathring{A}$, respectively. We only considered SWCNTs due to the expected negligible effect of an outer CNT wall on the chemical reactions inside the inner tubes.[3]

Although the actual identity and composition of the carbonaceous precursors in the CNT is unknown (and probably comprises a heterogeneous mixture of carbon species) our choice of dicarbon molecules (C_2) is motivated by the well-known presence of these species in carbon vapor samples (as found in carbon stars, electric arcs, hydrocarbons flames, interstellar medium, comets, etc) giving rise to the so-called Swan spectral bands. Therefore, we started with an array of consecutive carbon dimers (C_2) and compared its time evolution under different SWCNT diameters (Fig.5). However, the starting configuration of the inner carbon array might introduce a bias in the subsequent dynamics. To rule out this possibility, we adopted the following 3-steps setup procedure: (1) First, we generated a perfect polyyne carbon chain of similar length as the SWCNT used. (2) Then, we chopped the chain in random places by randomly removing C atoms from the array according to a uniform probability distribution. The result contains a series of carbonaceous segments of varying lengths (monomers, dimers, trimers, etc). To further eliminate any spatial bias, the coordinates of the remaining C atoms were displaced randomly according to a normalized Gaussian distribution with standard deviation of 0.1 angstroms in all 3 spatial directions. (3) The resulting array configuration was introduced inside the (6,4) SWCNT and the whole system was subjected to a brief geometry relaxation prior the MD run. The results were

similar as the one shown in Fig. 5. This robust and more general protocol mimics the experiment to some extent: at high temperatures, one expects the presence of many carbon segments of varying length (albeit with a different probability distribution of segments). The existence of such nucleating segments (or "seeds") inside the SWCNT has the further advantage of facilitating the subsequent self-assembly during the MD simulations. The distribution of the length of the initial carbon segments present inside the CNT's is unknown and beyond the scope of this study.

The whole system (SWCNT+inner carbon chain) was centered in a cubic box of volume 366.84^3 $\mathring{A}^3$, large enough to avoid interactions between the xy lateral periodic images. No thermostats were used to avoid altering the natural dynamics of the system, therefore, all the MD simulations proceeded in the microcanonical ensemble (NVE) to explore the intrinsic dynamical behavior of the system without the perturbing effect of thermostats. The initial ionic velocities were drawn from a Maxwell-Boltzmann distribution at 700 K and other temperatures used in our experimental setup. The MD time step was 0.25 fs. The simulation covered a total of 150 ps, and we output snapshots every 100 fs. In the movie of supporting information, adjacent snapshots are separated by 200 fs.

References

1. Stuart, S. J.; Tutein, A. B.; Harrison, J. A. A reactive potential for hydrocarbons with intermolecular interactions. J. Chem. Phys. **2000**, 112, 6472–6486.

2. Plimpton, S. Fast parallel algorithms for short-range molecular dynamics. J. Comput. Phys. **1995**, 117, 1–19.

3. Shi, L.; Yanagi, K.; Cao, K.; Kaiser, U.; Ayala, P.; Pichler, T. Extraction of Linear Carbon Chains Unravels the Role of the Carbon Nanotube Host. ACS Nano **2018**, 12, 8477–8484.

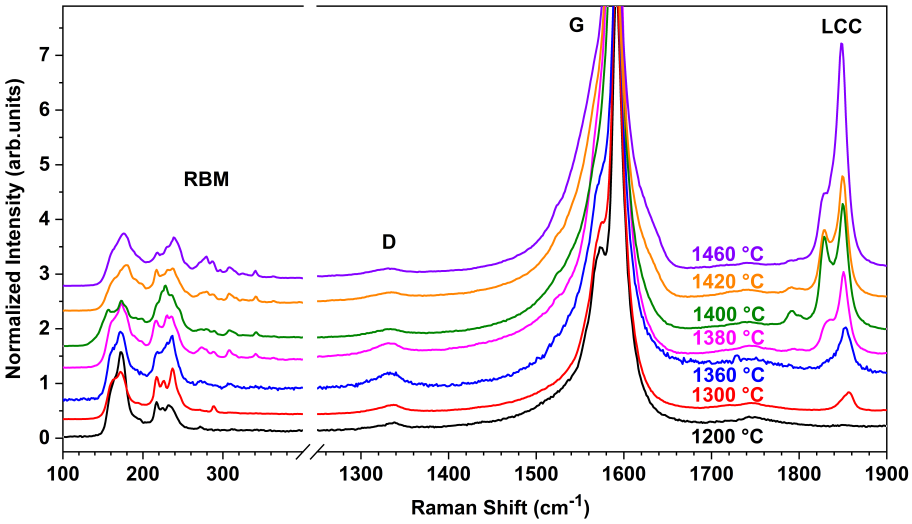

Fig. S1: Raman spectra of the annealed eDIPS-1.3 nm SWCNTs at different temperatures excited by a laser with wavelength of 568 nm.

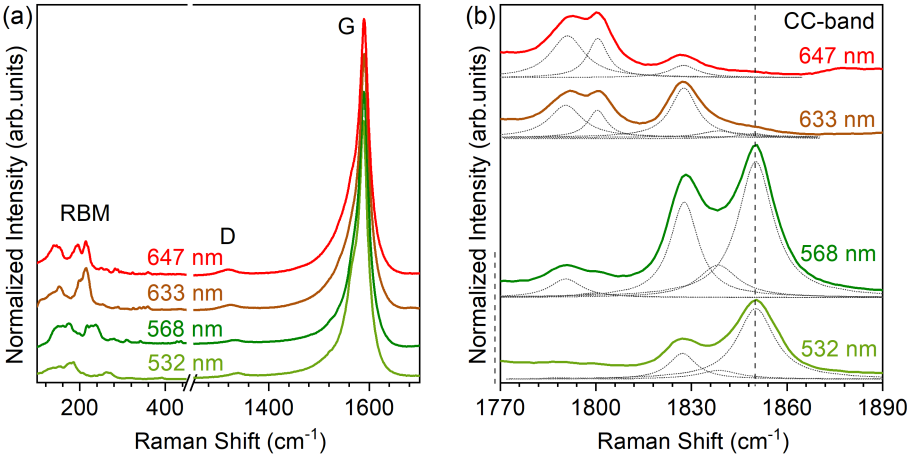

Fig. S2: Raman spectra of the annealed eDIPS-1.3 nm SWCNTs at 1460 °C excited by multi-frequency lasers with wavelengths of 532, 568, 633, and 647 nm.

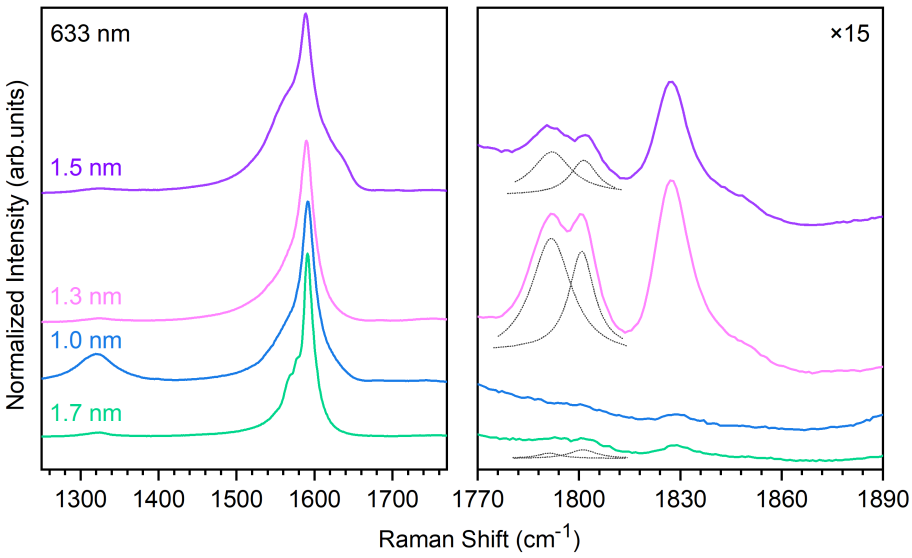

Fig. S3: Raman spectra of the annealed eDIPS-1.0 nm, eDIPS-1.3 nm, eDIPS-1.7 nm SWCNTs and DWCNTs-1.5 nm excited by a laser with wavelength of 633 nm.

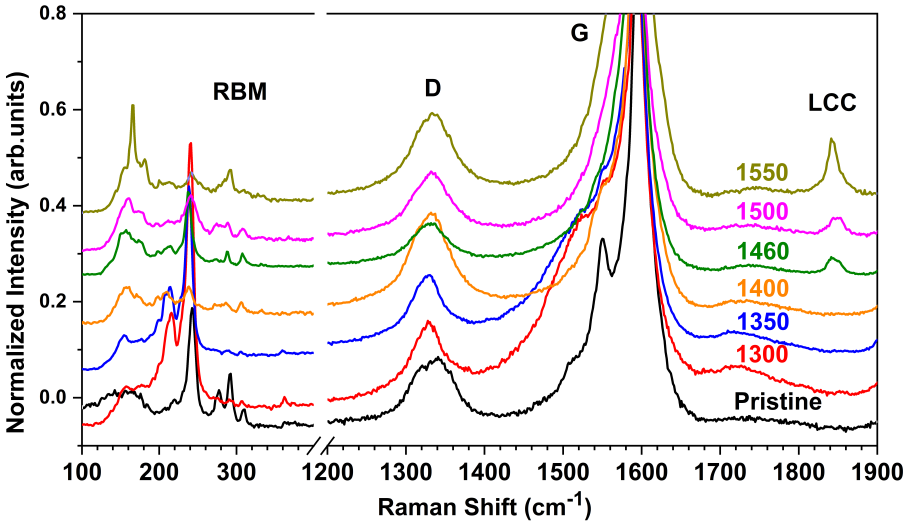

Fig. S4: Raman spectra of the annealed eDIPS-1.0 nm SWCNTs at different temperatures excited by a laser with wavelength of 568 nm.

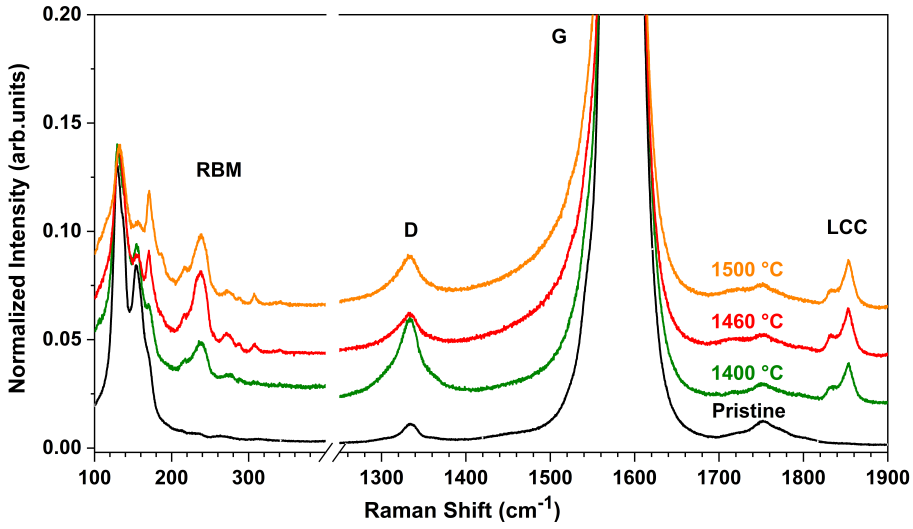

Fig. S5: Raman spectra of the annealed eDIPS-1.7 nm SWCNTs at different temperatures excited by a laser with wavelength of 568 nm.

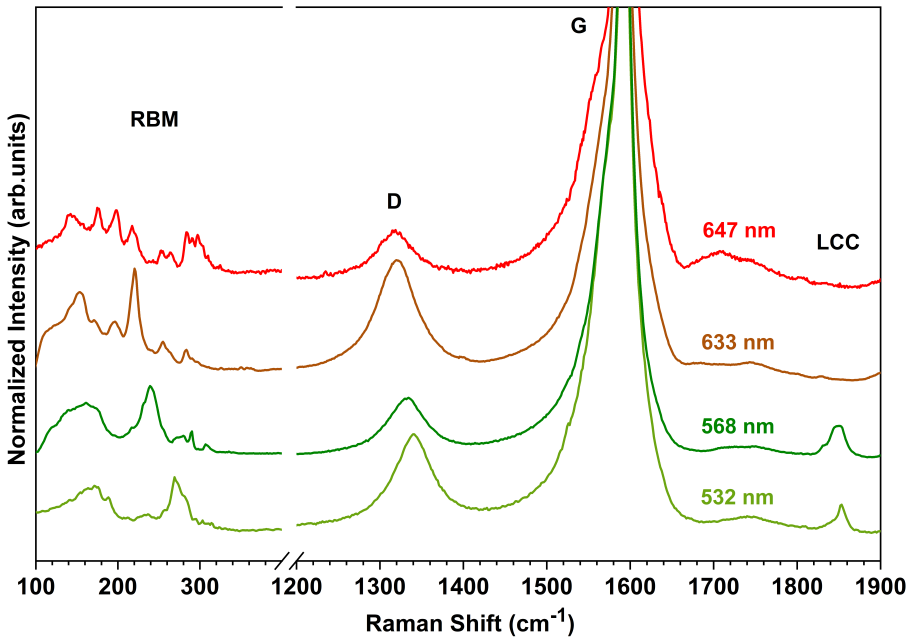

Fig. S6: Raman spectra of the annealed eDIPS-1.0 nm SWCNTs at 1500 °C excited by multi-frequency lasers with wavelengths of 532, 568, 633, and 647 nm.

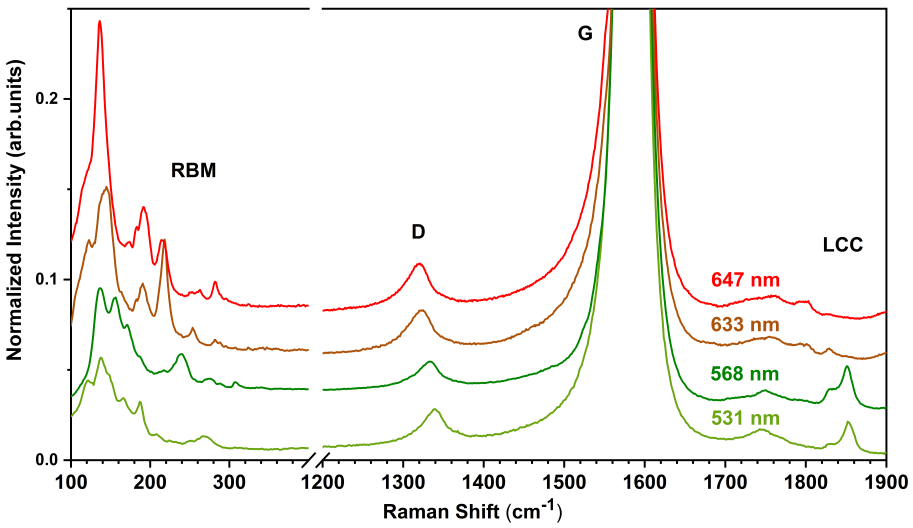

Fig. S7: Raman spectra of the annealed eDIPS-1.7 nm SWCNTs at 1460 °C excited by multi-frequency lasers with wavelengths of 532, 568, 633, and 647 nm.

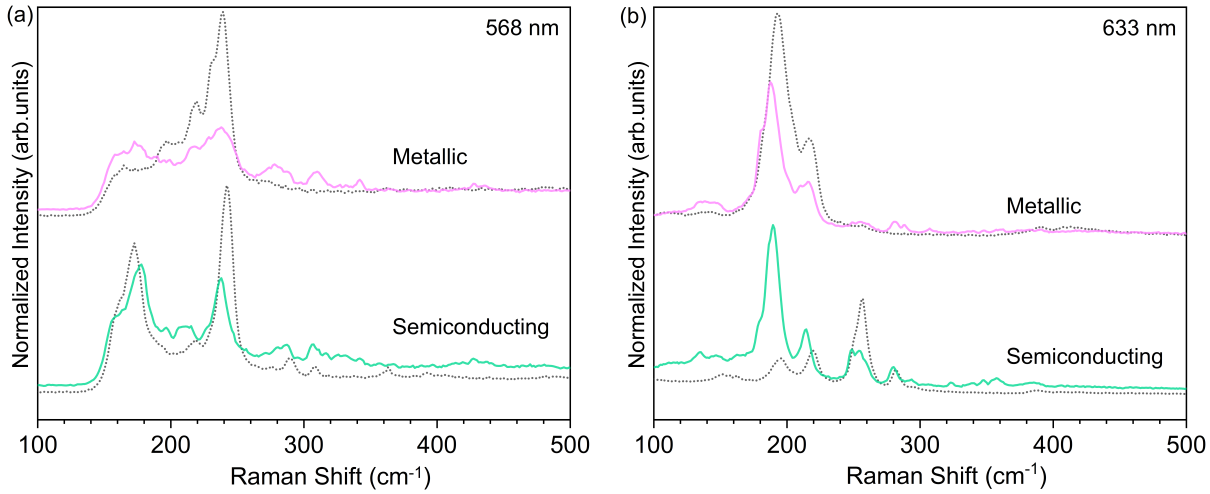

Fig. S8: RBM of the annealed metallic and semiconducting SWCNTs at 1460 °C excited by lasers with wavelengths of 568 and 633 nm.